Mild Hydrothermal Crystal Growth of Two Luminescing Uranyl Phosphates Exhibiting an Autunite-type Sheet Structure

Gopabandhu Panigrahi, Mark D. Smith, and Hans-Conrad zur Loye*

Department of Chemistry and Biochemistry, University of South Carolina, Columbia, SC, 29208, United States

*E-mail: zurloye@mailbox.sc.edu

ABSTRACT: Two new layered uranyl phosphate compounds, $K(UO_2)PO_4(H_2O)_3$ and $Na(UO_2)PO_4(H_2O)_{1.52}$, crystallizing in an autunite-type sheet structure, were successfully synthesized as both single-crystals and polycrystalline powders under mild hydrothermal conditions. The compound $K(UO_2)PO_4(H_2O)_3$ crystallizes in the tetragonal crystal system with the space group *P*4/*ncc***,** exhibiting lattice parameters of $a = b = 6.99320(7)$ Å and $c = 17.8389(3)$ Å. Similarly, $Na(UO_2)PO_4(H_2O)_{1.52}$ also crystallizes in the tetragonal crystal system, however in the space group *P*4/*nmm* and exhibits lattice parameters of $a = b = 6.9787$ Å and $c = 8.6303(17)$ Å. Both compounds adopt layered structures, a characteristic feature of uranyl phosphates, and exhibit intense green fluorescence typical for uranyl-containing materials. The infrared spectroscopy, photoluminescence and scintillation properties of these compounds were investigated.

Introduction:

The need to immobilize radioactive waste in durable waste forms capable of safely enduring for thousands of years has been a critical consideration since the inception of nuclear technology. As the production of nuclear energy and associated waste continues to grow, the development of effective and reliable containment strategies has become increasingly urgent. Radioactive waste typically contains radionuclides that remain hazardous for extensive periods of time, necessitating materials capable of providing long-term isolation by limiting the mobility of the radionuclides to prevent environmental contamination.[1] Researchers are actively exploring novel materials and methods to address these challenges, with a growing focus on actinide compounds, including uranyl-based materials, due to their unique chemical and physical properties. Uranyl compounds exhibit rich structural chemistry and also hold significant potential for a variety of applications, including proton conductivity, catalysis, photochemistry, non-linear optical materials, light emitting phosphor, ion exchange and X-ray scintillators.[2–10] Additionally, uranyl compounds, such as uranyl phosphates, have garnered considerable attention as they naturally occur in uranium deposits and, thus, can help in understanding the mobility of uranium in natural systems.[11–14]

The structural diversification of uranium phosphates arises from the incorporation of various additional metals, including alkali metals, alkaline earth metals, and lanthanides. This incorporation leads to the formation of a wide array of structural motifs, as these metals can influence the coordination environment, dimensionality, and connectivity of the uranium phosphate framework.[15–18] Despite their promising properties, the number of known actinide phosphate compounds remains relatively small, leaving considerable room for the discovery of new materials. Recent advances in synthesis techniques have facilitated the exploration of uranyl phosphates. Many of these compounds have been synthesized using mild hydrothermal reactions and flux crystal growth methods, both of which offer excellent control over material formation.[19–24] The hydrothermal synthesis approach is particularly versatile, as it allows researchers to produce a wide range of uranyl compounds by varying parameters such as temperature, pressure, and pH.[22,25] This method has proven effective in creating materials with tailored properties and expanding the possibilities for developing waste forms optimized for specific radionuclides.

Among the many materials under investigation, layered phosphates have emerged as particularly promising candidates for addressing the challenges of nuclear waste immobilization.

We report the synthesis, structural characterization, and physicochemical properties of two novel uranyl phosphate compounds: sodium uranyl phosphate, $Na(UO_2)PO_4(H_2O)_{1.52}$, and potassium uranyl phosphate, $K(UO_2)PO_4(H_2O)_3$. These compounds were synthesized using mild hydrothermal conditions, yielding high-quality crystals. Both structures adopt a layered autunite-type topology, characterized by the arrangement of uranyl phosphate sheets separated by interlayer sodium or potassium cations and water molecules. Notably, the interlayer species exhibit positional disorder. Herein we present a comprehensive analysis of the synthesis routes, single-crystal and powder X-ray diffraction studies, elemental composition verified through energy-dispersive spectroscopy (EDS), thermal stability, infrared spectroscopy, and their scintillation and fluorescence properties.

Experimental

$UO_2(CH_3CO_2)2.2H_2O$ (International Bio-Analytical Industries, ACS grade), Na_2CO_3 (Fisher scientific) K_2CO_3 (BDH), $NaBF_4$ (Alfa Aesar, 97%), KBF_4 ((Alfa Aesar, 98%), KH_2PO_4 (Fisher scientific), $Na_2HPO_4.7H_2O$ (Fisher scientific)

Caution: Although the uranium precursors used contain depleted uranium, standard safety procedures for handling radioactive materials must be followed.

For the synthesis of $K(UO_2)PO_4(H_2O)_3$, a mixture of 30 mg of K_2CO_3, 20 mg of $UO_2(CH_3CO_2)_2{\cdot}2H_2O$, 30 mg of KBF_4, and 20 mg of KH_2PO_4 was combined with 5 mL of deionized water in a 23 mL polytetrafluoroethylene (PTFE) liner. Similarly, for the synthesis of $Na(UO_2)PO_4(H_2O)_{1.52}$, 30 mg of Na_2CO_3, 20 mg of $UO_2(CH_3CO_2)_2{\cdot}2H_2O$, 30 mg of $NaBF_4$, and 20 mg of Na_2HPO_4 were mixed with 5 mL of deionized water in the 23 mL PTFE liner. The tetrafluoroborate and carbonate salts were primarily utilized as sources of alkali metals. In addition to serving as alkali metal sources, the carbonate salts play a crucial role in suppressing the formation and precipitation of uranyl fluorides by forming soluble complexes with uranium species.

In both cases, the PTFE liner containing the reaction mixture was sealed inside a stainless-steel autoclave and placed in a programmable oven. The reaction mixtures were initially heated to 200 °C over a period of 2 hours, maintained at 200 °C for 48 hours to allow crystallization, and then gradually cooled to 30 °C at a controlled rate of 5 °C per hour. Upon completion of the reactions, the autoclaves were opened, revealing light green crystals of the desired compounds. The mother liquor was carefully decanted to separate it from the solid product. The crystals were then isolated by vacuum filtration and thoroughly washed with deionized water to remove any residual impurities, yielding the final, high-purity products suitable for further analysis. The semiquantitative EDS analyses were performed using single crystals of both these compound to characterize the elemental composition.

We performed several reactions to produce phase pure compounds in bulk quantity by optimizing the same reaction conditions. Nonetheless, the PXRD patterns of the powder samples of $K(UO_2)PO_4(H_2O)_3$ and $Na(UO_2)PO_4(H_2O)_{1.52}$ indicate the presence of very minor impurities.

X-Ray Structure Determination, $K(UO_2)PO_4(H_2O)_3$

X-ray intensity data from a light green square plate were collected at 303(2) K using a Bruker D8 QUEST diffractometer equipped with a PHOTON-II area detector and an Incoatec microfocus source (Mo Kα radiation, λ = 0.71073 Å). The data collection covered 99.8% of reciprocal space to $2\theta_{max}$ = 60.0º, with an average reflection redundancy of 40.2 and R_{int} = 0.049 after absorption correction. The raw area detector data frames were reduced and corrected for absorption effects using the SAINT+ and SADABS programs.[26,27] Final unit cell parameters were determined by least-squares refinement of 9863 reflections taken from the data set. An initial structural model was obtained with SHELXT. Subsequent difference Fourier calculations and full-matrix least-squares refinement against F^2 were performed with SHELXL-2019/3 using ShelXle.[29]

The compound crystallizes in the tetragonal system. The space group *P*4/*ncc* was uniquely determined by the pattern of systematic absences in the intensity data and was confirmed by the structure solution. The asymmetric unit consists of one uranium atom, one phosphorus atom, three pure oxygen atom sites and one mixed potassium / water oxygen site. Atoms U1, O1 and O2 are located on four-fold rotational axes (site 4*c*), atom P1 is located on a -4 axis (site 4*b*) and atoms O3 and O4/K1 are located on general positions (site 16*g*). The mixed O4/K1 was initially refined as 100% oxygen. The O4/K1 mixed site occupancy was identified by refinement of the O4 site occupancy, which refined to > 100% O (*ca*. 137%), but to less than 100% K. In accordance with elemental analysis results, which found potassium in the crystals, this site was refined as a mixed O/K site. The constrained refinement resulted in 74.0% O / 26.0 % K, which was subsequently fixed at 75% O / 25% K to maintain electroneutrality. No other atomic site showed a significant deviation from full occupancy. All atoms were refined with anisotropic displacement parameters. Hydrogen atoms could not be located and were not calculated for the disordered water O4. The largest residual electron density peak and hole in the final difference map are +1.16 and -2.45 $e^-/Å^3$, located 1.50 Å from O3 and 0.53 Å from U1.

X-Ray Structure Determination, $Na(UO_2)PO_4(H_2O)_{1.52}$

X-ray intensity data from a green block were collected at 297(2) K using a Bruker D8 QUEST diffractometer equipped with a PHOTON-II area detector and an Incoatec microfocus source (Mo Kα radiation, λ = 0.71073 Å). The data collection covered 99.6% of reciprocal space to $2\theta_{max}$ = 65.3º, with an average reflection redundancy of 29.0 and R_{int} = 0.056 after absorption

correction. The raw area detector data frames were reduced and corrected for absorption effects using the SAINT+ and SADABS programs.[26,27] Final unit cell parameters were determined by least-squares refinement of 9958 reflections taken from the data set. An initial structural model was obtained with SHELXT.[28] Subsequent difference Fourier calculations and full-matrix least-squares refinement against F^2 were performed with SHELXL-2019/3[3] using ShelXle.[29]

The compound crystallizes in the tetragonal system. The space group *P*4/*nmm* was consistent with the pattern of systematic absences in the intensity data and was confirmed by structure solution. The asymmetric unit consists of one uranium atom, one phosphorus atom, three pure oxygen atom sites and a disordered layer modeled with sodium and oxygen atoms. Atoms U1, O1 and O2 are located on site 4*c* with *4*mm site symmetry; atom P1 is located on site 2*b* with -4*m*2 symmetry and atom O3 is located on a mirror plane (site 8*i*, *.m*. symmetry). Between the 2D layers generated by atoms U1, P1, O1-O3, several disordered electron density peaks were observed, of which three dominated. These were modeled as mixed sodium / oxygen atoms of variable occupancy, with the oxygen atoms presumed to be from water molecules. Initially several additional peaks were added, but most refined to near zero occupancy. The three major peaks remaining were at first refined as mixed Na/O sites, but this proved unstable, with two refining to 100% Na and one refining to 100 % O. For the final model, Na1 (site symmetry 4*mm*) and Na2 and O4 (general positions, site 16*k*) were assigned a fixed isotropic displacement parameter of 0.045 Å^2 (1.5 times the average U_{eq} of the other atoms). The sodium site occupancies were initially refined freely, giving a composition of $Na_{0.9}UO_2PO_4$, but were subsequently constrained to satisfy charge balance. The O4 occupancy was refined freely. No other atomic site showed a significant deviation from full occupancy. All other atoms were refined with anisotropic displacement parameters. Hydrogen atoms could not be located and were not calculated for the disordered water O4. The largest residual electron density peak and hole in the final difference map are +3.33 and -2.30 e$^-$/Å^3, both < 1 Å from U1.

Table 1. Crystallographic information of $Na(UO_2)PO_4(H_2O)_{1.52}$ and $K(UO_2)PO_4(H_2O)_3$

Formula	$K(UO_2)PO_4(H_2O)_3$	$Na(UO_2)PO_4(H_2O)_{1.52}$
Formula weight	452.10	412.28
Temperature	303(2) K	297(2) K
Wavelength	0.71073 Å	
Crystal system	Tetragonal	
Space group	*P*4/*ncc*	*P*4/*nmm*
Unit cell dimensions	a = 6.99320(7) Å	a = 6.9787(10) Å
	b = 6.99320(7) Å	b = 6.9787(10) Å
	c = 17.8389(3) Å	c = 8.6303(17) Å
Volume	872.41(2) $Å^3$	420.32(15) $Å^3$
Z	4	2
Density (calculated)	3.442 Mg/m^3	3.258 Mg/m^3
Absorption coefficient	19.281 mm^{-1}	19.543 mm^{-1}
F(000)	792	356
Reflections collected	31792	22946
Independent reflections	643 [R(int) = 0.0488]	482 [R(int) = 0.0559]
Completeness to theta = 25.242°	99.8 %	99.6 %
Max. and min. transmission	0.0990 and 0.0346	0.4950 and 0.3609
Refinement method	Full-matrix least-squares on F^2	Full-matrix least-squares on F^2
Data / restraints / parameters	643 / 0 / 31	482 / 1 / 28
Goodness-of-fit on F^2	1.253	1.228
Final R indices [I>2sigma(I)]	R1 = 0.0284, wR2 = 0.1202	R1 = 0.0220, wR2 = 0.0538
Largest diff. peak and hole	1.158 and -2.447 e.$Å^{-3}$	3.331 and -2.304 e.$Å^{-3}$

Powder X-ray Diffraction (PXRD).

Powder X-ray diffraction (PXRD) data were obtained by analyzing finely ground powder samples of $Na(UO_2)PO_4(H_2O)_{1.52}$ and $K(UO_2)PO_4(H_2O)_3$ crystals synthesized by using the mild hydrothermal synthesis method. PXRD data were collected on a Bruker D2 PHASER diffractometer using Cu-Kα radiation (λ = 1.5418 Å) over the 2θ range 5-65° with a step size of 0.02°.

Energy-Dispersive X-Ray Spectroscopy (EDS).

EDS data were collected on single crystals of $Na(UO_2)PO_4(H_2O)_{1.52}$ and $K(UO_2)PO_4(H_2O)_3$ by mounting them directly onto a SEM stub using conducting carbon tape. Quantitative elemental analysis was performed utilizing a Tescan Vega-3 SEM instrument, which was fitted with a Thermo EDS attachment. The SEM operated in a low-vacuum mode with a 15-20 kV accelerating voltage and a 40-second accumulation time. The summarized SEM results can be found in the supporting information (Table S1). The SEM pictures of $Na(UO_2)PO_4(H_2O)_{1.52}$ and $K(UO_2)PO_4(H_2O)_3$ crystals are shown in Figure1a and 1b, respectively.

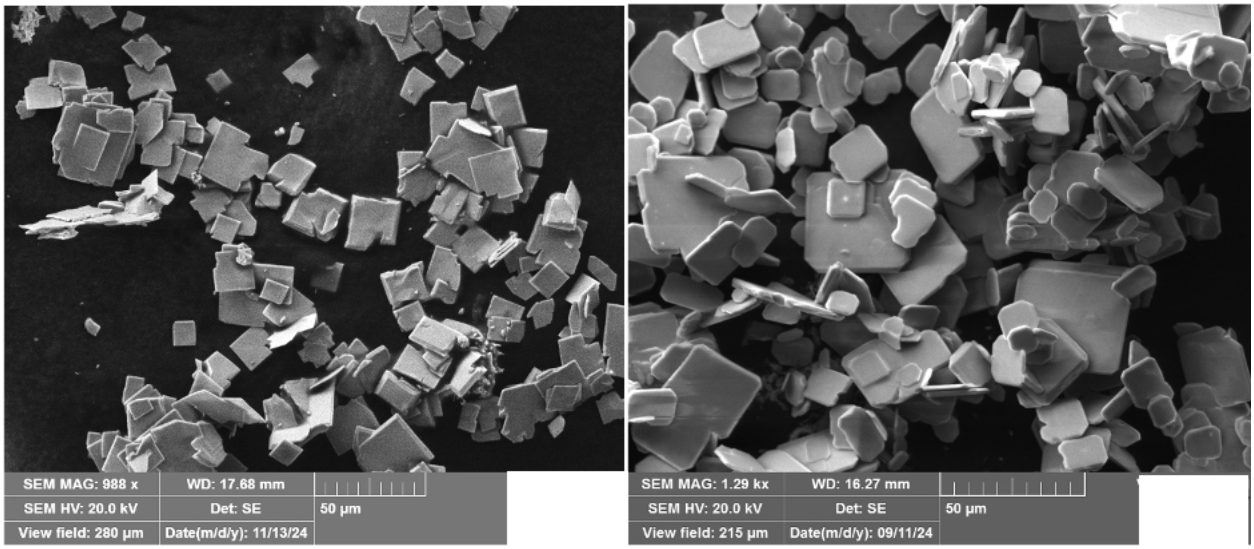

Figure 1. (a) The SEM image of $Na(UO_2)PO_4(H_2O)_{1.52}$ and **(b)** $K(UO_2)PO_4(H_2O)_3$ crystals

Photoluminescence.

Photoluminescence data were collected using a HORIBA scientific microscope spectroscopy system, equipped with a HORIBA iHR320 imaging spectrograph and a Synapse CCD detector. A confocal 375 nm diode laser was used as the excitation source. Data acquisition

was performed with LabSpec 6 software over the 400−800 nm range, utilizing a 10.0 mW laser power and a 10× UV objective.

Infrared spectroscopy:

Infrared (IR) spectroscopy measurements were conducted using a Perkin-Elmer Spectrum 100 FT-IR spectrometer equipped with a diamond attenuated total reflectance (ATR) attachment. The spectra were collected over a broad spectral range of 4000–650 cm^{-1} to capture characteristic vibrational modes of the sample. Each final spectrum represents an average of 16 individual scans, ensuring improved signal-to-noise ratio and reproducibility of the recorded data.

Result and discussion:

Crystal Structure

We successfully synthesized two layered compounds, $Na(UO_2)PO_4(H_2O)_{1.52}$ and $K(UO_2)PO_4(H_2O)_3$, using a mild hydrothermal synthesis method. Both compounds crystallize in the tetragonal crystal system, with space groups *P*4/*nmm* for $Na(UO_2)PO_4(H_2O)_{1.52}$ and *P*4/*ncc* for $K(UO_2)PO_4(H_2O)_3$ and exhibit an autunite-type sheet structure. The autunite-type sheet structure is quite distinct from other common uranyl phosphate layer structures, such as the well-known phosphuranylite family of structures, which consists of chains of uranyl pentagonal or hexagonal bipyramids that are linked by phosphate groups that decorate the edges of the chains.[16,20,30]

The $K(UO_2)PO_4(H_2O)_3$ compound is isostructural with the previously reported $K(UO_2)PO_4(D_2O)_3$. The $K(UO_2)PO_4(D_2O)_3$ structure was refined from neutron and synchrotron X-ray powder diffraction data.[31,32] For the first time we synthesized single crystals of $Na(UO_2)PO_4(H_2O)_{1.52}$ and $K(UO_2)PO_4(H_2O)_3$ by using the mild hydrothermal synthesis method and explored their physical properties. The EDS analysis of $Na(UO_2)PO_4(H_2O)_{1.52}$ crystals indicates the presence of Na, U, P, and O and of K, U, P, and O in $K(UO_2)PO_4(H_2O)_3$ crystals. The elemental compositions of these crystals are listed in Table S1. The PXRD patterns collected using polycrystalline powder samples of $Na(UO_2)PO_4(H_2O)_{1.52}$ and $K(UO_2)PO_4(H_2O)_3$ are shown in Figures 2 and Figure S1.

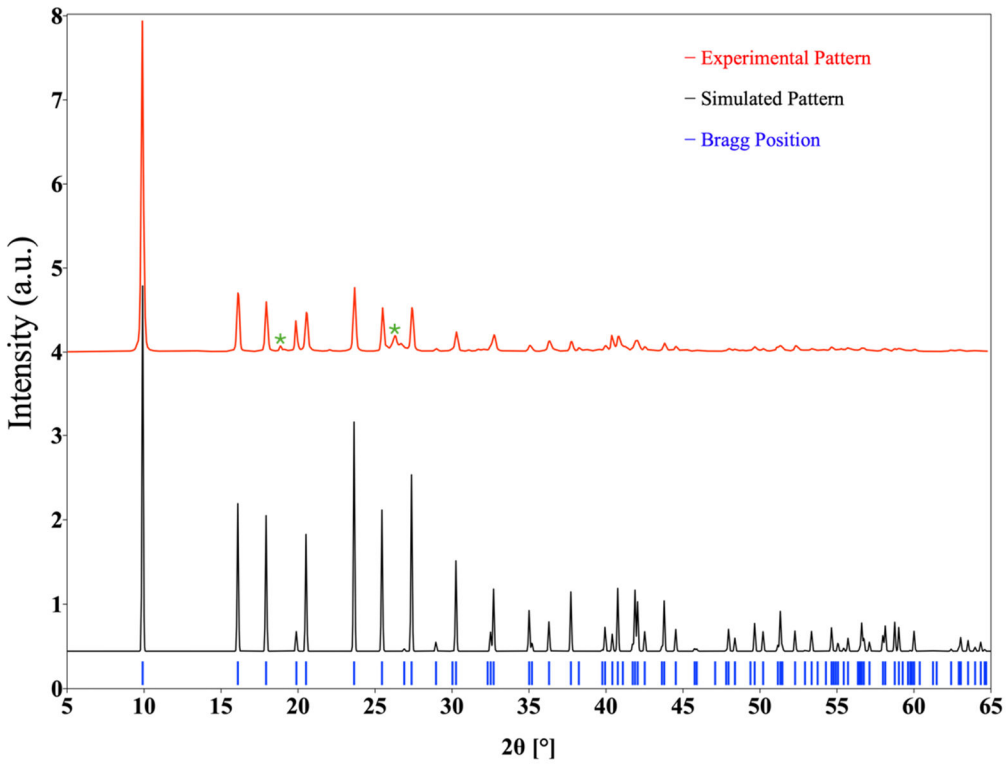

Figure 2. The PXRD pattern of polycrystalline $K(UO_2)PO_4(H_2O)_3$ compound (simulated pattern (black) experimental pattern (red) and Bragg position (blue)) (* presence of minor impurities)**.**

The crystal structure of $K(UO_2)PO_4(H_2O)_3$ is shown in Figures 3a and 3b, and features two-dimensional uranyl phosphate sheets of the autunite-type, that are formed by vertex sharing between phosphate tetrahedra and uranyl square bipyramids.[1] The $K(UO_2)PO_4(H_2O)_3$ structure contains seven different atomic sites, one uranium, one potassium, one phosphorus, and four oxygen sites, which create $^{\infty}_{2}[(UO)_2PO_4]^-$ sheets that are separated by disordered K^+ ions and H_2O molecules occupying the interlayer spaces (Figure 3a and 3b). The disorder is characterized by 25% K and 75% O occupying the same atomic site between the two dimensional $^{\infty}_{2}[(UO)_2PO_4]^-$ sheet. The structure comprises octahedral UO_6 units and tetrahedral PO_4 groups, which form the autunite-type uranyl phosphate sheets (Figure 3c). Each UO_6 octahedron shares the four equatorial vertices with four surrounding PO_4 tetrahedra, resulting in the robust autunite-type sheet structure (Figure 3d). Isolated UO_6 polyhedra, connected via intervening PO_4 units, where the uranyl oxygens extend above and below the plane of the sheet. The details of crystallographic data, interatomic distances, and other crystallographic details are given in Table 1 and Tables S2-S4.

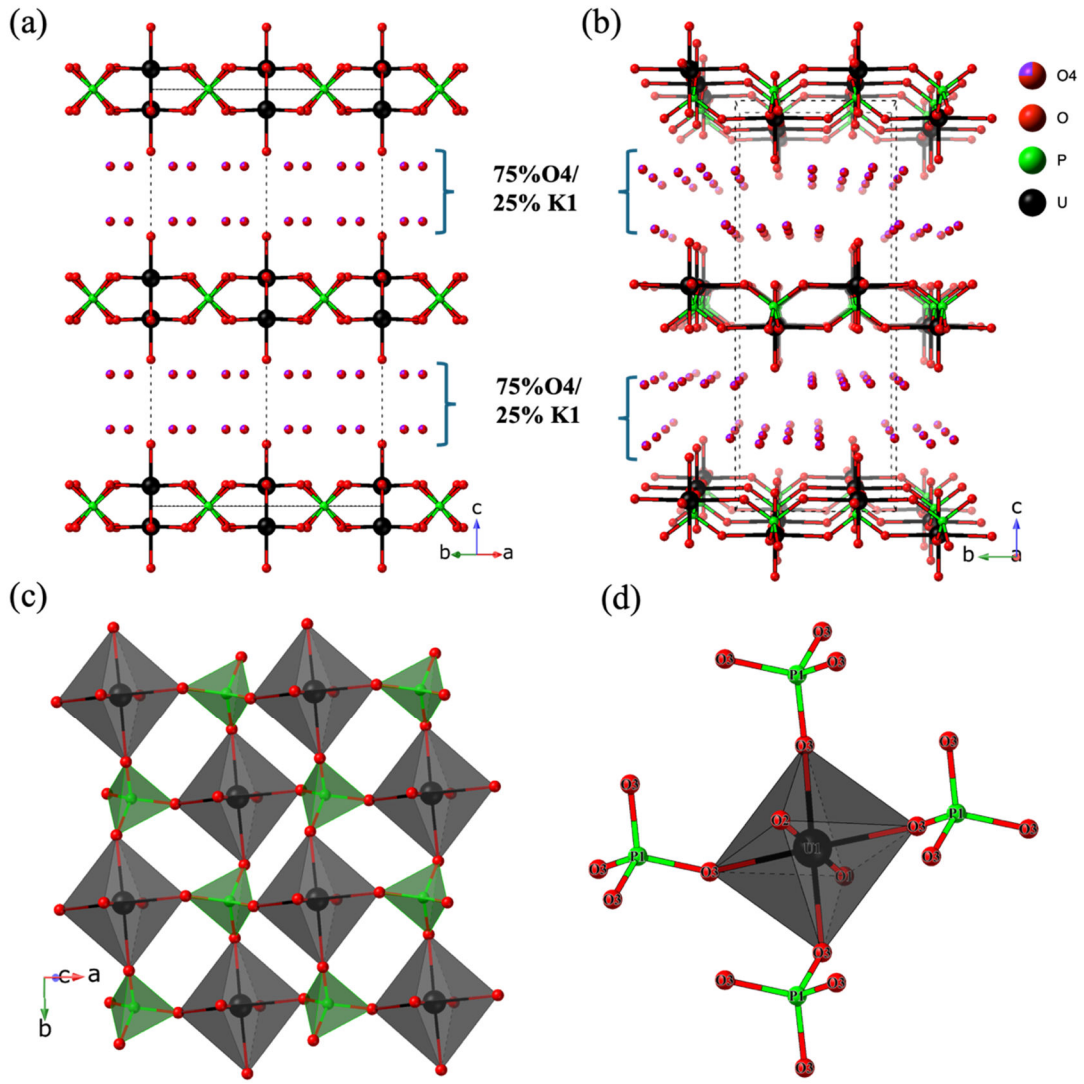

Figure 3. The **(a)** and **(b)** unit cell representation of $K(UO_2)PO_4(H_2O)_3$ along [110] and *a*-direction, **(c)** polyhedral view $^{\infty}_{2}[(UO)_2PO_4]^-$ sheet, **(d)** vertex sharing of PO_4 tetrahedra units with UO_6 polyhedra through O3.

Similarly, the $Na(UO_2)PO_4(H_2O)_{1.52}$ structure (Figure 4a) also consists of two-dimensional autunite-type uranyl phosphate sheets. The $Na(UO_2)PO_4(H_2O)_{1.52}$ compound contain eight different atomic sites one uranium, two sodium, one phosphorus, and four oxygen sites. In this compound, the interlayer spacing contains disordered Na^+ ions and H_2O molecules, which occupy different atomic sites (Figure 4b). The connectivity within the two dimensional $^{\infty}_{2}[(UO)_2PO_4]^-$ uranyl phosphate sheets, where UO_6 octahedra share four equatorial vertices with adjacent PO_4 tetrahedra, is identical to that observed in $K(UO_2)PO_4(H_2O)_3$. The only difference in the

$Na(UO_2)PO_4(H_2O)_{1.52}$ structure is in the interlayer space, which contain disordered Na and O atoms. There are two different disordered Na atoms present in the interlayer space with site

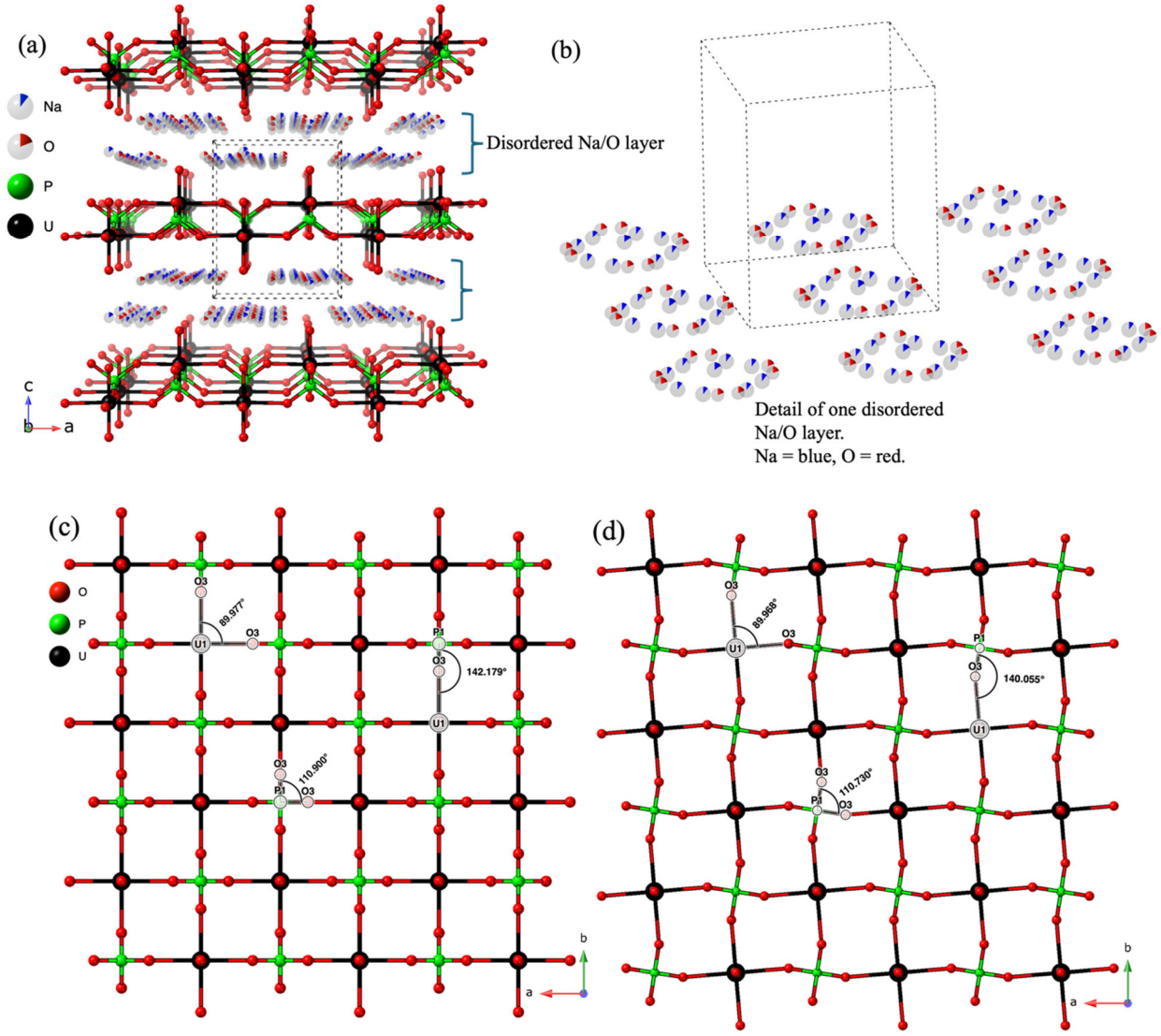

Figure 4. The **(a)** unit cell representation of $Na(UO_2)PO_4(H_2O)_{1.52}$ along *b*-direction, **(b)** detail of one disordered Na/O layer (Na-blue and O-red), (c) and (d) two dimensional $^{\infty}_{2}[(UO)_2PO_4]^-$ autunite-type sheet of $Na(UO_2)PO_4(H_2O)_{1.52}$ and $K(UO_2)PO_4(H_2O)_3$ along [110] direction.

occupancy of 15.6% (Na1) and 10.6% (Na2). The oxygen (O4) present in the interlayer spacing has a site occupancy of 19%. Figures 4c and 4d illustrate the two-dimensional $^{\infty}_{2}[(UO)_2PO_4]^-$ autunite-type sheet structure present in $Na(UO_2)PO_4(H_2O)_{1.52}$ and $K(UO_2)PO_4(H_2O)_3$. The $^{\infty}_{2}[(UO)_2PO_4]^-$ sheets in both compounds exhibit a similar layered topology; however, the structural arrangement in $K(UO_2)PO_4(H_2O)_3$ compound appears to be more disordered. This

increased disorder may be attributed to the presence of K^+ ions in the interlayer region which, due to their larger ionic radius compared to Na^+, likely induce greater structural perturbations and weaker interlayer interactions. Furthermore, while the O3–U–O3 and O3–P–O3 bond angles remain nearly identical in both compounds, a notable difference is observed in the PO_4 and UO_6 polyhedra tilt angles, which is noticeably greater in $K(UO_2)PO_4(H_2O)_3$ than in $Na(UO_2)PO_4(H_2O)_{1.52}$ (Figure 4 c,d). The details of the crystallographic data, interatomic distances, and other crystallographic details are given in Table 1 and Tables S5-S7.

The uranyl square bipyramidal (UO_6) units in $Na(UO_2)PO_4(H_2O)_{1.52}$ are representative of the typical uranyl polyhedra, exhibiting two short uranyl bonds (1.767(8) and 1.801(9)) and four long equatorial bonds (4 x 2.274(5)). The bond distances are essentially the same as those in $K(UO_2)PO_4(H_2O)_3$, where the UO_6 square bipyramid exhibits two short uranyl bonds (1.784(14) and 1.788(13)) and four long equatorial bonds (4 x 2.281(6)). These distances are consistent with the bond lengths observed in structurally related uranyl compounds reported in the literature, suggesting that the uranium-oxygen bonding in these systems adheres to typical structural norms.[33–35]

The PO_4 bond lengths, on the other hand, exhibit slight differences between the two compounds. In $K(UO_2)PO_4(H_2O)_3$, the PO_4 bond length is 1.541(5) Å, whereas in $Na(UO_2)PO_4(H_2O)_{1.52}$, it is slightly shorter at 1.516(5) Å. These observed differences in bond lengths may arise due to variations in the hydration levels and the influence of the alkali metal cations (Na^+ versus K^+), which affect the local coordination environment and bonding interactions. Overall, the bond lengths in both UO_6 and PO_4 units are within the expected ranges for similar compounds, reflecting their structural integrity and stability.[19,20,36,37]

Photoluminescence:

The photoluminescence properties of $Na(UO_2)PO_4(H_2O)_{1.52}$ and $K(UO_2)PO_4(H_2O)_3$ suggest that the emission is highly sensitive to the local coordination environment surrounding the uranium atom. Factors such as the geometry, bond lengths, and interactions with neighboring atoms within the coordination unit can influence the d−f or f−f electronic transitions that give rise to luminescence. This sensitivity underscores the importance of the crystal structure in determining the optical properties of uranium-based materials, making them interesting for further study and

potential application in luminescent technologies. Figure 5 presents the fluorescence emission spectra for the $Na(UO_2)PO_4(H_2O)_{1.52}$ and $K(UO_2)PO_4(H_2O)_3$ compound when excited at 375 nm. The emission spectrum exhibits characteristic features typical of uranyl-containing compounds,[38] displaying a series of well-defined peaks. Specifically, the spectrum consists of six distinct emission bands centered at 485 nm, 501 nm, 522 nm, 545 nm, 574 nm, and 600 nm. We did not observe any difference or major shift of the peaks in the fluorescence emission spectra of $Na(UO_2)PO_4(H_2O)_{1.52}$ and $K(UO_2)PO_4(H_2O)_3$, as both contain the same two dimensional $^{\infty}_{2}[(UO)_2PO_4]^-$ sheet having essentially identical uranium coordination environments.

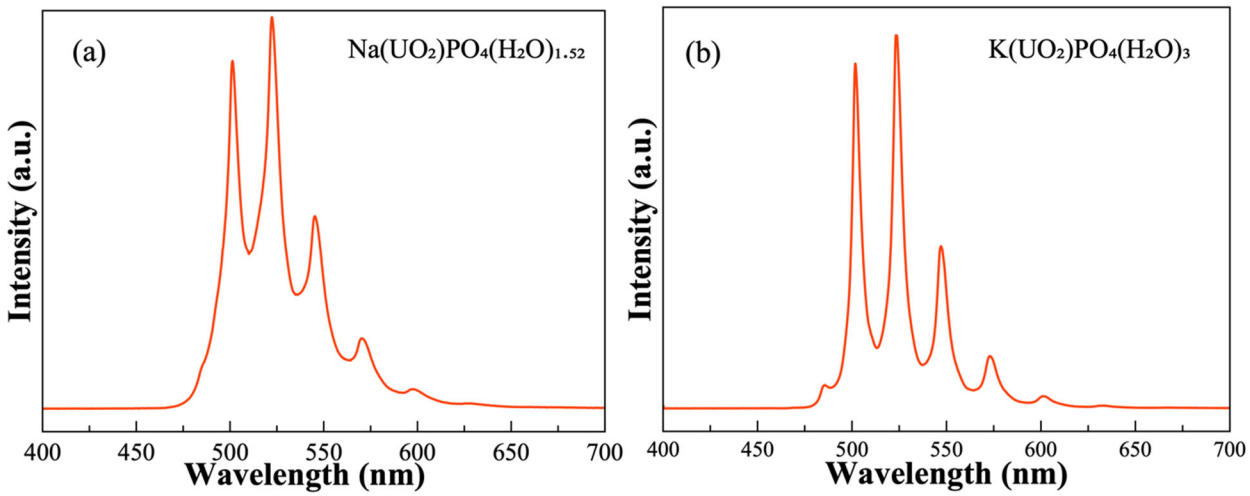

Figure 5. Fluorescence emission spectra of (a) $Na(UO_2)PO_4(H_2O)_{1.52}$ and (b) $K(UO_2)PO_4(H_2O)_3$ excited at 375 nm.

To further evaluate the functional properties of $Na(UO_2)PO_4(H_2O)_{1.52}$ and $K(UO_2)PO_4(H_2O)_3$, its scintillation behavior was examined. When illuminated with Cu X-rays, the crystals exhibited a bright green scintillation (Figure 6a and 6b). This confirms the material's ability to act as a scintillator, converting high-energy X-ray photons into visible light emissions. The green scintillation is characteristic of the $Na(UO_2)PO_4(H_2O)_{1.52}$ and $K(UO_2)PO_4(H_2O)_3$ compounds and reflects their capability to support fast radiative transitions. Such scintillation properties are particularly valuable in applications such as radiation detection, medical imaging, and high-energy physics instrumentation.

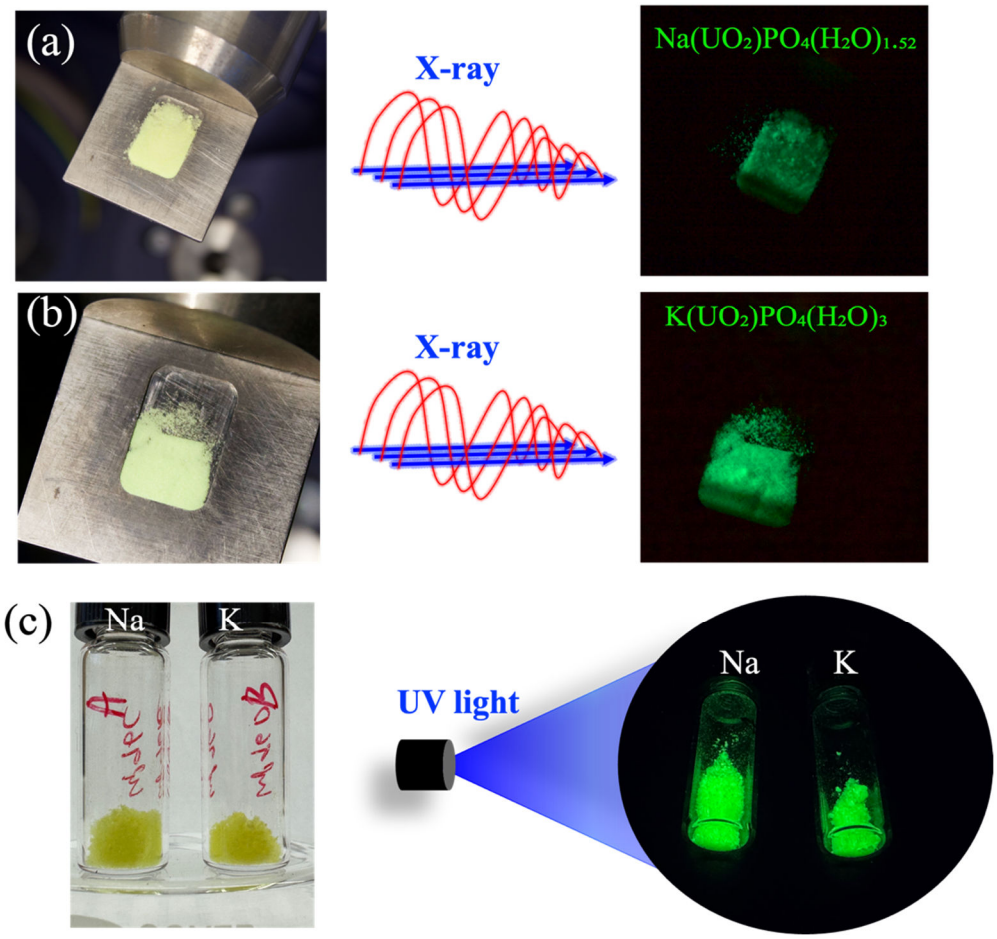

Figure.6 Scintillation of (a) $Na(UO_2)PO_4(H_2O)_{1.52}$, and (b) $K(UO_2)PO_4(H_2O)_3$ under X-ray illumination and (c) fluorescence image of $Na(UO_2)PO_4(H_2O)_{1.52}$, and (b) $K(UO_2)PO_4(H_2O)_3$ under UV-light illumination.

Additionally, the material demonstrated luminescence under short wavelength ultraviolet (UV) light (Figure 6c), highlighting the versatility of $Na(UO_2)PO_4(H_2O)_{1.52}$ and $K(UO_2)PO_4(H_2O)_3$ in responding to different excitation sources, suggesting potential use in optical applications.

Thermal Analysis:

The weight loss behavior of $K(UO_2)PO_4(H_2O)_3$ during heating is depicted in Figure 7, illustrating the thermal decomposition profile of the compound. The thermogravimetric analysis (TGA) reveals a total weight loss of approximately 11% over the temperature range of 25 °C to 500 °C. This observed mass reduction is attributed to the release of water molecules from the crystal structure. Given that the theoretical contribution of the three water molecules (H_2O) in $K(UO_2)PO_4(H_2O)_3$ accounts for approximately 11.8% of the total mass, the measured weight loss aligns closely with the expected dehydration process.

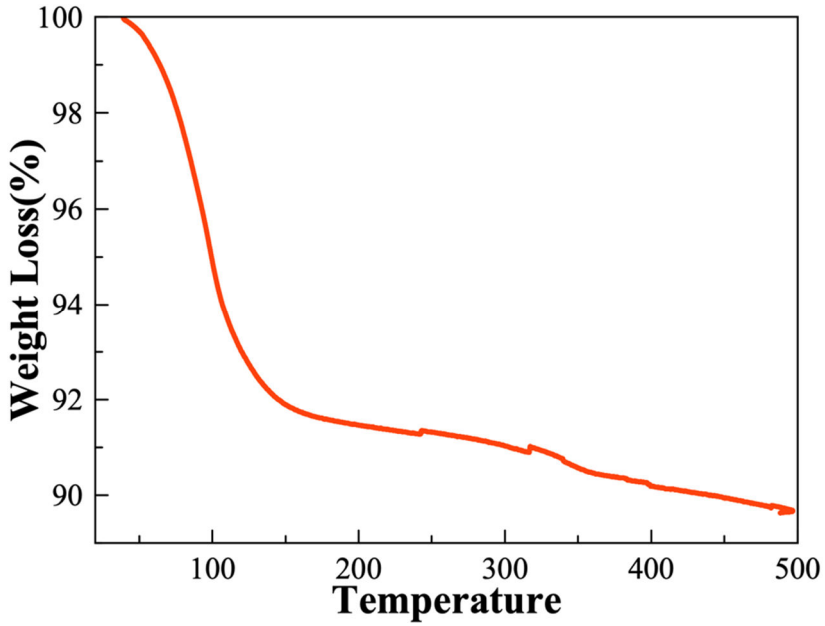

Figure.7 TGA plot of $K(UO_2)PO_4(H_2O)$ under nitrogen gas flow.

Infrared spectroscopy:

The Fourier-transform infrared (FTIR) spectra of $Na(UO_2)PO_4(H_2O)_{1.52}$ and $K(UO_2)PO_4(H_2O)_3$ are presented in Figure 8, providing insights into the vibrational modes of these compounds. A distinct absorption band observed around ~3400 cm^{-1} corresponds to the stretching vibration of hydroxyl (O-H) groups, which can be attributed to the presence of water molecules in the crystal structure. Additionally, a bending vibration mode of the O-H groups appears at approximately ~1600 cm^{-1}, further confirming the presence of molecular water in these phases. The broad and intense absorption bands centered around 1000 cm^{-1} is evident for all phases, which is characteristic of the P-O stretching modes associated with the phosphate groups.

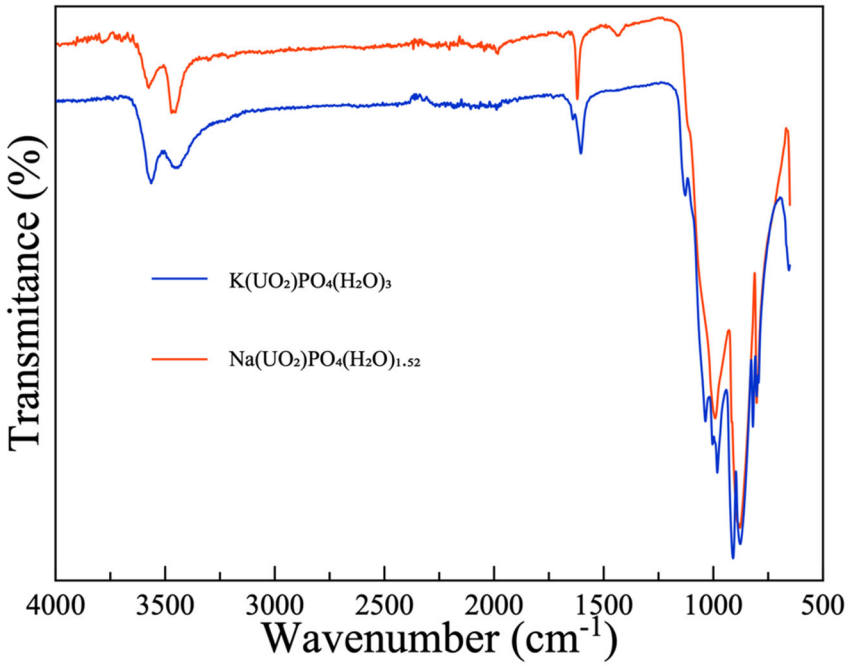

Figure.8 Infrared spectroscopy data for $K(UO_2)PO_4(H_2O)_3$ (bottom) and $Na(UO_2)PO_4(H_2O)_{1.52}$ (top).

Conclusion:

Two layered uranyl phosphate compounds, $K(UO_2)PO_4(H_2O)_3$ and $Na(UO_2)PO_4(H_2O)_{1.52}$, have been successfully synthesized under mild hydrothermal conditions in both single-crystal and polycrystalline forms. Structural characterization revealed that both compounds crystallize in the tetragonal crystal system, with $K(UO_2)PO_4(H_2O)_3$ belonging to the P4/ncc space group and $Na(UO_2)PO_4(H_2O)_{1.52}$ adopting the P4/nmm space group. The lattice parameters for $K(UO_2)PO_4(H_2O)_3$ are a = b = 6.99320(7) Å, c = 17.8389(3) Å, while $Na(UO_2)PO_4(H_2O)_{1.52}$ exhibits lattice parameters of a = b = 6.9787 Å and c = 8.6303(17) Å. Both compounds feature layered structural motifs typical of uranyl phosphates and display the intense green luminescence characteristic of uranyl-containing materials. Additionally, the scintillation behavior of polycrystalline $Na(UO_2)PO_4(H_2O)_{1.52}$, and $K(UO_2)PO_4(H_2O)_3$ was evaluated under X-ray illumination.

Notes
The authors declare no competing financial interest.

Associated Content

Supporting Information

The supporting information includes EDS tabulated data, PXRD patterns, and tables of atomic parameters and bond lengths. This information is available free of charge at the website XXX

The CCDC 2421769-2421770 entries encompass the supplementary crystallographic data associated with this paper. These data are accessible without charge through www.ccdc.cam.ac.uk/data_request/cif, or by sending a request via email to data_request@ccdc.cam.ac.uk, or by directly contacting The Cambridge Crystallographic Data Centre at 12 Union Road, Cambridge CB2 1EZ, UK; fax: +44 1223 336033. The supporting information (SI) file contains EDS results, TGA plots, and PXRD patterns of title compounds.

ACKNOWLEDGMENTS

The authors gratefully acknowledge the support from the U.S. Department of Energy, Office of Basic Energy Sciences, Division of Materials Sciences and Engineering, under award DE-SC0018739. Synthesis, structural characterization, thermal property and photoluminescent studies were conducted at the University of South Carolina.

Reference:

(1) Locock, A. J.; Burns, P. C. The Crystal Structure of Synthetic Autunite, $Ca[(UO_2)(PO_4)]_2(H_2O)_{11}$. *Am. Mineral.* **2003**, *88* (1), 240–244.

(2) Ling, J.; Qiu, J.; Sigmon, G. E.; Ward, M.; Szymanowski, J. E. S.; Burns, P. C. Uranium Pyrophosphate/Methylenediphosphonate Polyoxometalate Cage Clusters. *J. Am. Chem. Soc.* **2010**, *132* (38), 13395–13402.

(3) Borkowski, L. A.; Cahill, C. L. Crystal Engineering with the Uranyl Cation I. Aliphatic Carboxylate Coordination Polymers: Synthesis, Crystal Structures, and Fluorescent Properties. *Cryst. Growth Des.* **2006**, *6* (10), 2241–2247.

(4) Adelani, P. O.; Albrecht-Schmitt, T. E. Differential Ion Exchange in Elliptical Uranyl Diphosphonate Nanotubules. *Angew. Chem. Int. Ed.* **2010**, *49* (47), 8909–8911.

(5) Grohol, D.; Subramanian, M. A.; Poojary, D. M.; Clearfield, A. Synthesis, Crystal Structures, and Proton Conductivity of Two Linear-Chain Uranyl Phenylphosphonates. *Inorg. Chem.* **1996**, *35* (18), 5264–5271.

(6) Knope, K. E.; Cahill, C. L. Homometallic Uranium(VI) Phosphonoacetates Containing Interlayer Dipyridines. *Inorg. Chem.* **2009**, *48* (14), 6845–6851.

(7) Wang, S.; Alekseev, E. V.; Ling, J.; Liu, G.; Depmeier, W.; Albrecht-Schmitt, T. E. Polarity and Chirality in Uranyl Borates: Insights into Understanding the Vitrification of Nuclear Waste and the Development of Nonlinear Optical Materials. *Chem. Mater.* **2010**, *22* (6), 2155–2163.

(8) Liao, Z.-L.; Li, G.-D.; Bi, M.-H.; Chen, J.-S. Preparation, Structures, and Photocatalytic Properties of Three New Uranyl−Organic Assembly Compounds. *Inorg. Chem.* **2008**, *47* (11), 4844–4853.

(9) Wang, X.; Song, E.; Qin, L.; Gui, D.; Xu, Z.; Xie, J.; Lei, M.; Zhang, H.; Wang, Y.; Wang, Y. Fabrication of a Wide Color Gamut Pc-WLED Surpassing 107% NTSC Based on a Robust Luminescent Uranyl Phosphate. *Chem. Mater.* **2021**, *33* (16), 6329–6337.

(10) Wang, Y.; Yin, X.; Liu, W.; Xie, J.; Chen, J.; Silver, M. A.; Sheng, D.; Chen, L.; Diwu, J.; Liu, N.; Chai, Z.; Albrecht-Schmitt, T. E.; Wang, S. Emergence of Uranium as a Distinct Metal Center for Building Intrinsic X-Ray Scintillators. *Angew. Chem.* **2018**, *130* (26), 8009–8013.

(11) zur Loye, H.-C.; Besmann, T.; Amoroso, J.; Brinkman, K.; Grandjean, A.; Henager, C. H.; Hu, S.; Misture, S. T.; Phillpot, S. R.; Shustova, N. B.; Wang, H.; Koch, R. J.; Morrison, G.; Dolgopolova, E. Hierarchical Materials as Tailored Nuclear Waste Forms: A Perspective. *Chem. Mater.* **2018**, *30* (14), 4475–4488.

(12) Guesdon, A.; Raveau, B. A New Uranium(VI) Monophosphate with a Layered Structure: $Ba_3[UO_2(PO_4)(PO_3(OH))]_2 \cdot xH_2O$ ($x \approx 0.4$). *Chem. Mater.* **1998**, *10* (11), 3471–3474.

(13) Oh, G. N.; Ringe, E.; Van Duyne, R. P.; Ibers, J. A. Synthesis, Structure, and Optical Properties of $CsU_2(PO_4)_3$. *J. Solid State Chem.* **2012**, *185*, 124–129.

(14) Keskar, M.; Vats, B.; Phatak, R.; Krishnan, K.; Sali, S.; Kannan, S. Structural and Thermal Studies of $SrU(PO_4)_2$ and $BaU(PO_4)_2$. *J. Alloys Compd.* **2017**, *725*, 1199–1209.

(15) Koo, H.-J.; Dai, D.; Whangbo, M.-H. Importance of Supersuperexchange Interactions in Determining the Dimensionality of Magnetic Properties. Determination of Strongly Interacting Spin Exchange Paths in $A_2Cu(PO_4)_2$ (A= Ba, Sr), $ACuP_2O_7$ (Ba, Ca, Sr, Pb), $CaCuGe_2O_6$, and $Cu_2UO_2(PO_4)_2$ on the Basis of Qualitative Spin Dimer Analysis. *Inorg. Chem.* **2005**, *44* (12), 4359–4365.

(16) Juillerat, C. A.; Moore, E. E.; Kocevski, V.; Besmann, T.; zur Loye, H.-C. A Family of Layered Phosphates Crystallizing in a Rare Geometrical Isomer of the Phosphuranylite Topology: Synthesis, Characterization, and Computational Modeling of $A_4[(UO_2)_3O_2(PO_4)_2]$ (A = Alkali Metal) Exhibiting Intralayer Ion Exchange. *Inorg. Chem.* **2018**, *57* (8), 4726–4738.

(17) Krivovichev, S.; Burns, P.; Tananaev, I. Crystal Chemistry of Actinide Phosphates and Arsenates. *Struct. Chem. Inorg. Actin. Compd.* **2006**, 217.

(18) Yang, W.; Wu, H.-Y.; Wang, R.-X.; Pan, Q.-J.; Sun, Z.-M.; Zhang, H. From 1D Chain to 3D Framework Uranyl Diphosphonates: Syntheses, Crystal Structures, and Selective Ion Exchange. *Inorg. Chem.* **2012**, *51* (21), 11458–11465.

(19) Usman, M.; Morrison, G.; Klepov, V. V.; Smith, M. D.; zur Loye, H.-C. Flux Crystal Growth, Structure, Magnetic and Optical Properties of a Family of Alkali Uranium(IV) Phosphates. *J. Solid State Chem.* **2019**, *270*, 19–26.

(20) Morrison, G.; Pace, K. A.; zur Loye, H.-C. Mild Hydrothermal Synthesis of Potassium Uranyl Phosphates with Layered and Framework Structures. *J. Solid State Chem.* **2021**, *301*, 122293.

(21) Shvareva, T. Y.; Albrecht-Schmitt, T. E. General Route to Three-Dimensional Framework Uranyl Transition Metal Phosphates with Atypical Structural Motifs: The Case Examples of $Cs_2\{(UO_2)_4[Co(H_2O)_2]_2(HPO_4)(PO_4)_4\}$ and $Cs^{3+x}[(UO_2)_3CuH_{4-x}(PO_4)_5]\cdot H_2O$. *Inorg. Chem.* **2006**, *45* (5), 1900–1902.

(22) Wylie, E. M.; Dawes, C. M.; Burns, P. C. Synthesis, Structure, and Spectroscopic Characterization of Three Uranyl Phosphates with Unique Structural Units. *J. Solid State Chem.* **2012**, *196*, 482–488.

(23) Locock, A. J.; Burns, P. C. Structures and Syntheses of Layered and Framework Amine-Bearing Uranyl Phosphate and Uranyl Arsenates. *J. Solid State Chem.* **2004**, *177* (8), 2675–2684.

(24) Alekseev, E. V.; Krivovichev, S. V.; Depmeier, W. Crystal Chemistry of Anhydrous Li Uranyl Phosphates and Arsenates. II. Tubular Fragments and Cation–Cation Interactions in the 3D Framework Structures of $Li_6[(UO_2)_{12}(PO_4)_8(P_4O_{13})]$, $Li_5[(UO_2)_{13}(AsO_4)_9(As_2O_7)]$, $Li[(UO_2)_4(AsO_4)_3]$ and $Li_3[(UO_2)_7(AsO_4)_5O)]$. *J. Solid State Chem.* **2009**, *182* (11), 2977–2984.

(25) Burns, P. C.; Alexopoulos, C. M.; Hotchkiss, P. J.; Locock, A. J. An Unprecedented Uranyl Phosphate Framework in the Structure of $[(UO_2)_3(PO_4)O(OH)(H_2O)_2](H_2O)$. *Inorg. Chem.* **2004**, *43* (6), 1816–1818.

(26) APEX3 Version 2019.1-0 and SAINT+ Version 8.40A. Bruker Nano, Inc., Madison, WI, USA, 2019.

(27) SADABS-2016/2: Krause, L., Herbst-Irmer, R., Sheldrick G.M. and Stalke D. J. Appl. Cryst. 2015, 48, 3-10.

(28)(A) SHELXT: Sheldrick, G.M. Acta Cryst. 2015, A71, 3-8. (b) SHELXL: Sheldrick, G.M. Acta Cryst. 2015, C71, 3-8.

(29)ShelXle: A Qt Graphical User Interface for SHELXL. Hübschle, C. B., Sheldrick, G. M., Bittrich, B. J. Appl. Cryst. 2011,.

(30)Juillerat, C. A.; zur Loye, H.-C. Crystal Growth and Structure Characterization of Three Layered Uranyl Phosphates and Their Relation to the Phosphuranylite Family. *Cryst. Growth Des.* **2018**, *19* (2), 1183–1189.

(31)Fitch, A. N.; Cole, M. The Structure of $KUO_2PO_{4.3}D_2O$ Refined from Neutron and Synchrotron-Radiation Powder Diffraction Data. *Mater. Res. Bull.* **1991**, *26* (5), 407–414.

(32)Cole, M.; Fitch, A. N.; Prince, E. Low-Temperature Structure of $KUO_2PO_{4\cdot3}D_2O$ Determined from Combined Synchrotron Radiation and Neutron Powder Diffraction Measurements. *J. Mater. Chem.* **1993**, *3* (5), 519–522.

(33)Ablott, T. A.; Lu, K. T.; Wei, T.; Zhang, Y. Exploring the Influence of pH on the Structural Intricacies of Uranium Oxide Hydrates Containing Both Cd(II) and K(I) Ions. *Dalton Trans.* **2023**, *52* (20), 6629–6640.

(34)Zhang, Y.; Lu, K. T.; Wei, T.; Karatchevtseva, I.; Zheng, R. Filling the Gaps of Uranium Oxide Hydrates with Magnesium(II) Ions: Unique Layered Structures and the Role of Additional Sodium(I) Ions. *Dalton Trans.* **2023**, *52* (47), 17942–17953.

(35)Morrison, G.; zur Loye, H.-C. Uranyl Titanate Silicates: Syntheses, Structures, and Family Relations. *Cryst. Growth Des.* **2022**, *22* (2), 1221–1228.

(36)Guesdon, A.; Provost, J.; Raveau, B. New Thorium and Uranium Monophosphates in the $KTh_2(PO_4)_3$ Family: Structure and Cationic Non-Stoichiometry. *J. Mater. Chem.* **1999**, *9* (10), 2583–2587.

(37)Wang, H.-Y.; Zheng, X.-Y.; Long, L.-S.; Kong, X.-J.; Zheng, L.-S. Sandwich-Type Uranyl Phosphate–Polyoxometalate Cluster Exhibiting Strong Luminescence. *Inorg. Chem.* **2021**, *60* (9), 6790–6795.

(38)Severance, R. C.; Vaughn, S. A.; Smith, M. D.; zur Loye, H.-C. Structures and Luminescent Properties of New Uranyl-Based Hybrid Materials. *Solid State Sci.* **2011**, *13* (6), 1344–1353.

For Table of Contents Use Only

Mild Hydrothermal Crystal Growth of Two Luminescing Uranyl Phosphates Exhibiting an Autunite-type Sheet Structure

Gopabandhu Panigrahi, Mark D. Smith, and Hans-Conrad zur Loye*

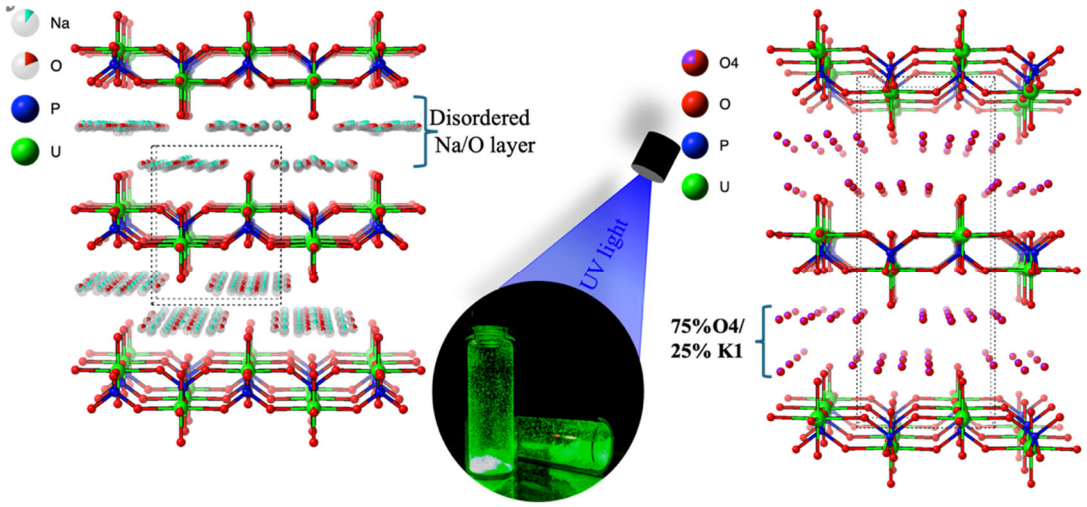

Two new layered luminescent uranyl phosphate compounds, $K(UO_2)PO_4(H_2O)_3$ and $Na(UO_2)PO_4(H_2O)_{1.52}$, were synthesized as both single-crystal and polycrystalline materials under mild hydrothermal conditions. These compounds crystallize in layered structures composed of two-dimensional $^{\infty}_{2}[(UO)_2PO_4]^-$ autunite-type sheets, which are separated by either Na^+ or K^+ cations along with interstitial water molecules. Both compounds exhibit intense green fluorescence under UV light excitation and demonstrate scintillation properties when exposed to X-ray radiation.